Supplementary Information

Supplementary Table 1: Summary of genome size, contigs and scaffolds of the phased genome assemblies.

Supplementary Table 2: Synteny and structural variations between two haplotypes of *R. breviuscula*.

Supplementary Fig. 1: Chromosome spreads and immunolocalisation in male *R. breviuscul*a meiocytes.

Supplementary Fig. 2: Dynamics of MLH1 during early prophase I in *R. breviuscula*.

Supplementary Fig. 3: Examples of ring bivalents with two foci (**a** and **c**) and rod bivalents with one focus (**b** and **d**) of MLH1 and HEI10 at diakinesis in *R. breviuscula*.

Supplementary Fig. 4: Cellranger clustering analysis of the 10X Genomics scRNA-seq of 2,528 pollen nuclei from *R. breviuscula*.

Supplementary Fig. 5: Selection of genotyping markers on the reference genome.

Supplementary Fig. 6: Pre-processing of scRNA-seq by separating *R. breviuscula* from *R. tenuis* cells and removing doublets.

Supplementary Fig. 7: Marker distribution on the reference and across all viable pollen nuclei.

Supplementary Fig. 8: Distance distribution of the first markers to the chromosome start and the last markers to the chromosome ends across all viable pollen nuclei.

Supplementary Fig. 9: Comparison of recombination frequencies in the single-pollen sequencing data and in the F_1 recombinant offspring of *R. breviuscula*.

Supplementary Fig. 10: CO interference on each chromosome.

Supplementary Fig. 11: Ka/Ks ratio estimation across the chromosomes of *R. breviuscula*.

Supplementary Fig. 12: Epigenetic regulation of repeat-based holocentromeres and fine-scale correlation of CO positions with *Tyba* repeats.

Supplementary Fig. 13: Comparison of numbers of COs overlapped with (epi)genetic features to random simulations.

Supplementary Fig. 14: Immunolocalisation of ASY1, ZYP1 and telomere-FISH.

Supplementary Fig. 15: Colocalization analysis of processed images of meiocytes at zygotene (top) and pachytene (bottom).

Supplementary Fig. 16: FISH with 35S rDNA and a telomeric probe in *R. breviuscula*.

Supplementary Table 1. Summary of genome size, contigs, and scaffolds of the phased genome assemblies.

	Haplotype 1	Haplotype 2
Genome assembly size (bp)	418,627,160	390,890,803
# Contigs	1637	548
Contig assembly size (bp)	421,256,472	391,742,506
Largest contig (bp)	35,313,519	43,961,622
Contig N50 (bp)	11,938,939	13,764,201
Contig N90 (bp)	42,248	2,739,863
# Scaffolds	1,501	457
Pseudo-chromosome size (bp)	368,174,147	370,478,156
Scaffold N50 (bp)	69,585,868	72,168,595
Scaffold N90 (bp)	45,843	66,381,717
Largest scaffold / chr 1 (bp)	91,632,052	89,220,796
Chromosome 2 (bp)	70,953,004	72,168,595
Chromosome 3 (bp)	69,585,868	69,956,709
Chromosome 4 (bp)	66,447,897	66,381,717
Chromosome 5 (bp)	69,555,326	72,750,339
Base accuracy (QV)	30.85	32.32
Completeness (%)	85	85
GC (%)	35.91	35.60

Supplementary Table 2. Synteny and structural variations between two haplotypes of *R. breviuscula*.

#Structural annotations			
#Variation_type	Count	Length hap1	Length hap2
Syntenic regions	229	329,130,991	329,924,075
Inversions	39	2,135,010	1,947,035
Translocations	346	3,620,755	3,569,626
Duplications (reference)	137	1,472,557	–
Duplications (query)	249	–	1168366
Not aligned (reference)	650	32,783,105	–
Not aligned (query)	808	–	33606738
#Sequence annotations			
#Variation_type	Count	Length hap1	Length hap2
SNPs	615,883	615883	615,883
Insertions	59,142	–	2,687,428
Deletions	59,276	3,101,459	–
Copy gains	87	–	126,950
Copy losses	60	394,961	–
Highly diverged	5,660	172,894,800	174,131,686
Tandem repeats	3	482	825

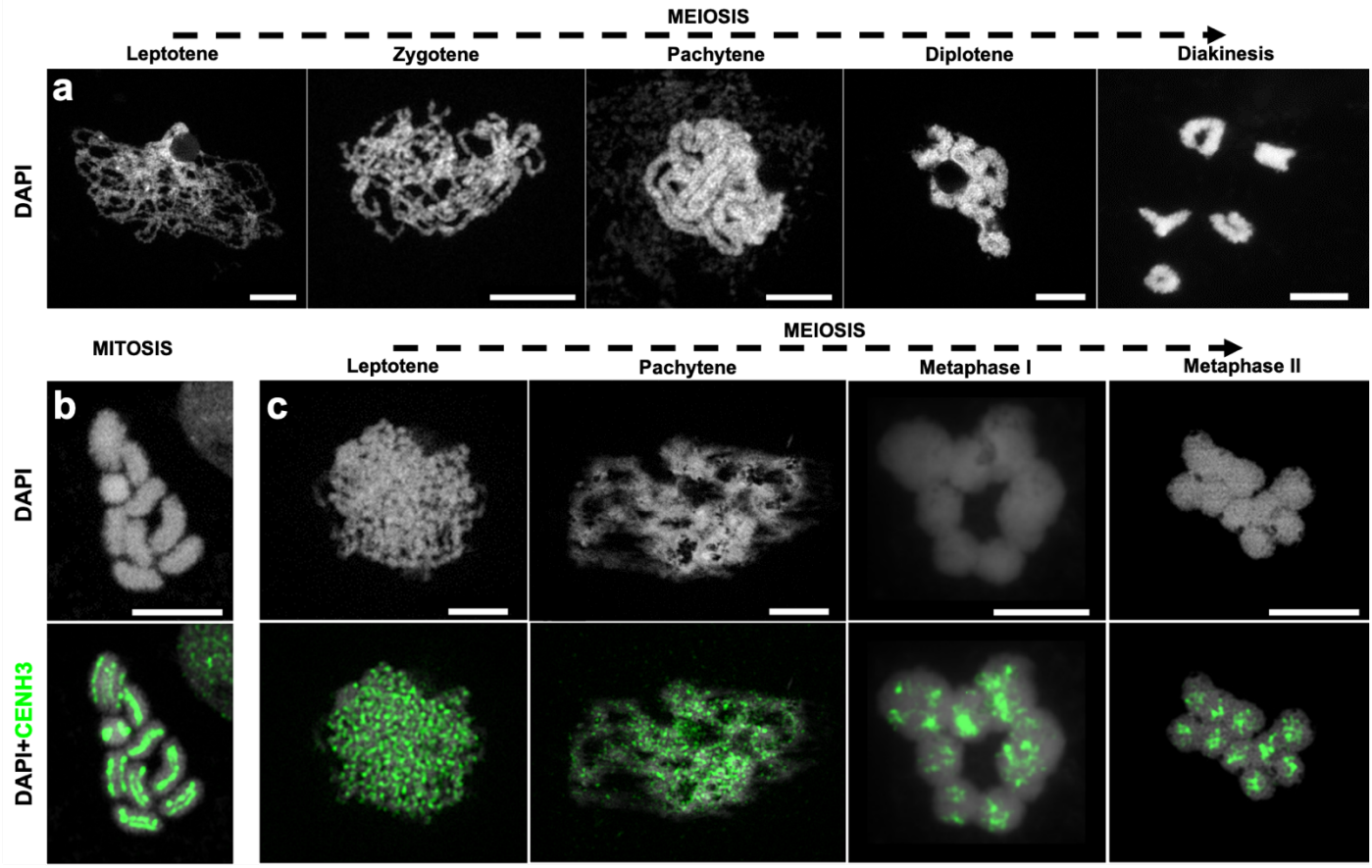

Supplementary Fig. 1: Chromosome spreads and immunolocalisation in male *R. breviuscula* meiocytes. (a) Meiotic stages are displayed, including leptotene, zygotene, pachytene, diplotene and diakinesis. **(b–c)** Immunolocalisation was performed against the centromeric protein CENH3, which appears as lines during mitosis **(b)** and as clusters during meiosis **(c)**. A maximum projection is shown, and the DNA was counterstained with DAPI. Scale bars, 5 µm.

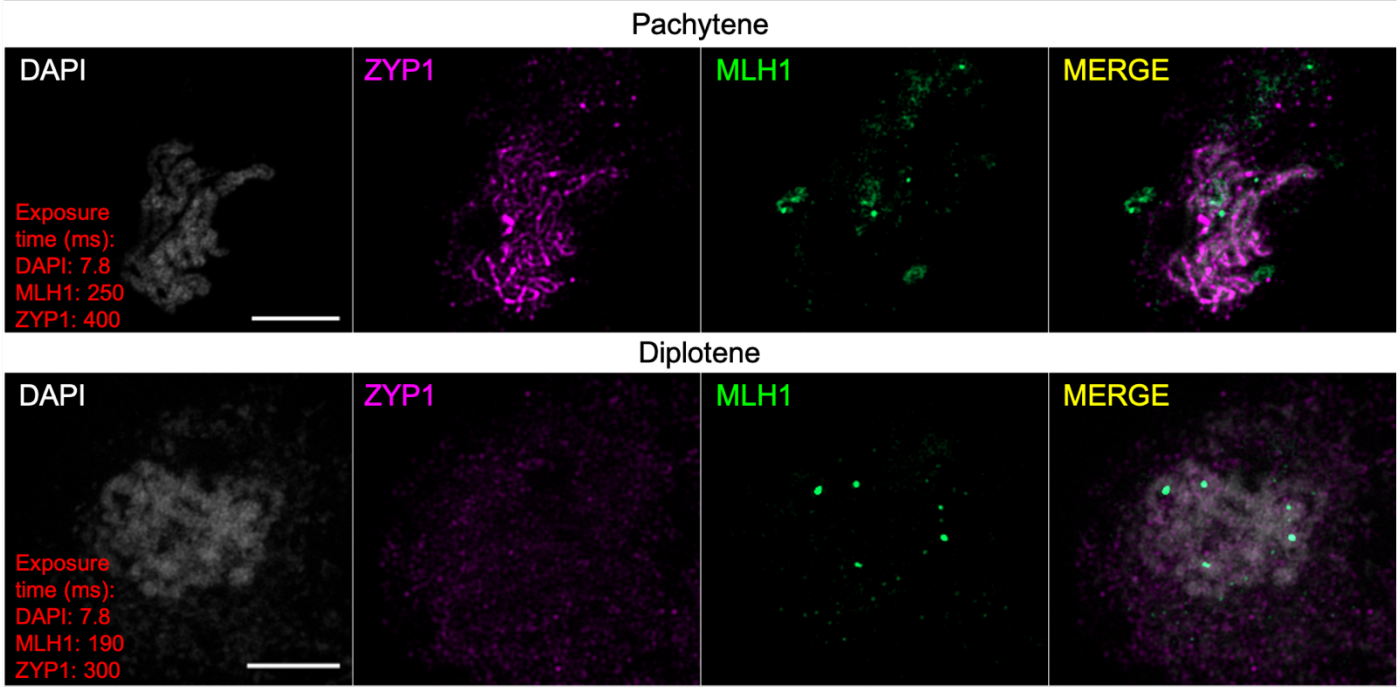

Supplementary Fig. 2: Dynamics of MLH1 during early prophase I in *R. breviuscula*. Note that MHL1 signals were never seen in early pachytene when ZYP1 signals were still present. MLH1 foci were only seen during diplotene and diakinesis when ZYP1 signals disappeared, representing the disassembly of the SC. Maximum projection is shown. DNA was counterstained with DAPI. Scale bar, 5um.

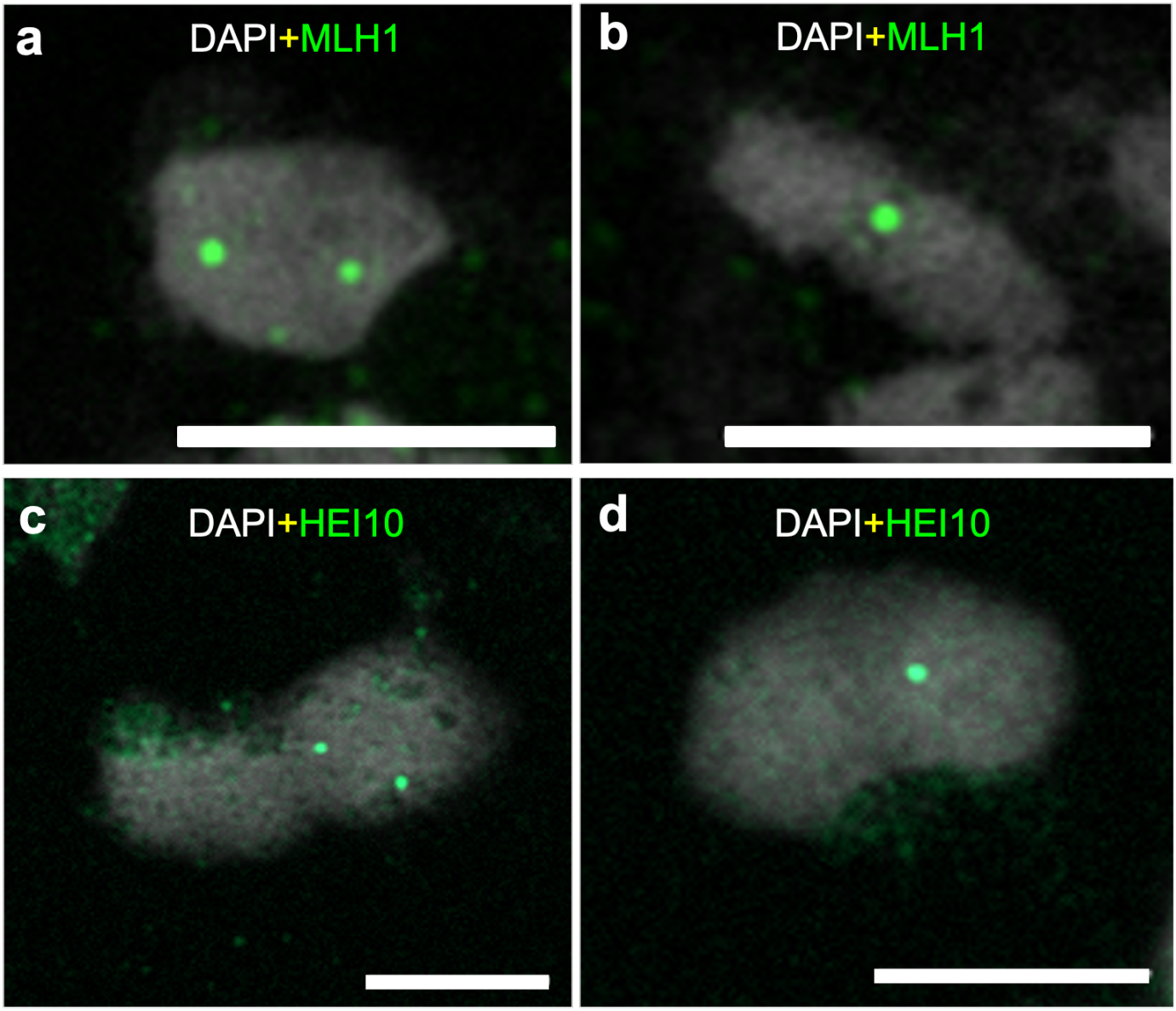

Supplementary Fig. 3: Examples of ring bivalents with two foci (a and c) and rod bivalents with one focus (b and d) of MLH1 and HEI10 at diakinesis in *R. breviuscula*. Maximum projection is shown. DNA was counterstained with DAPI. Scale bars, 5um.

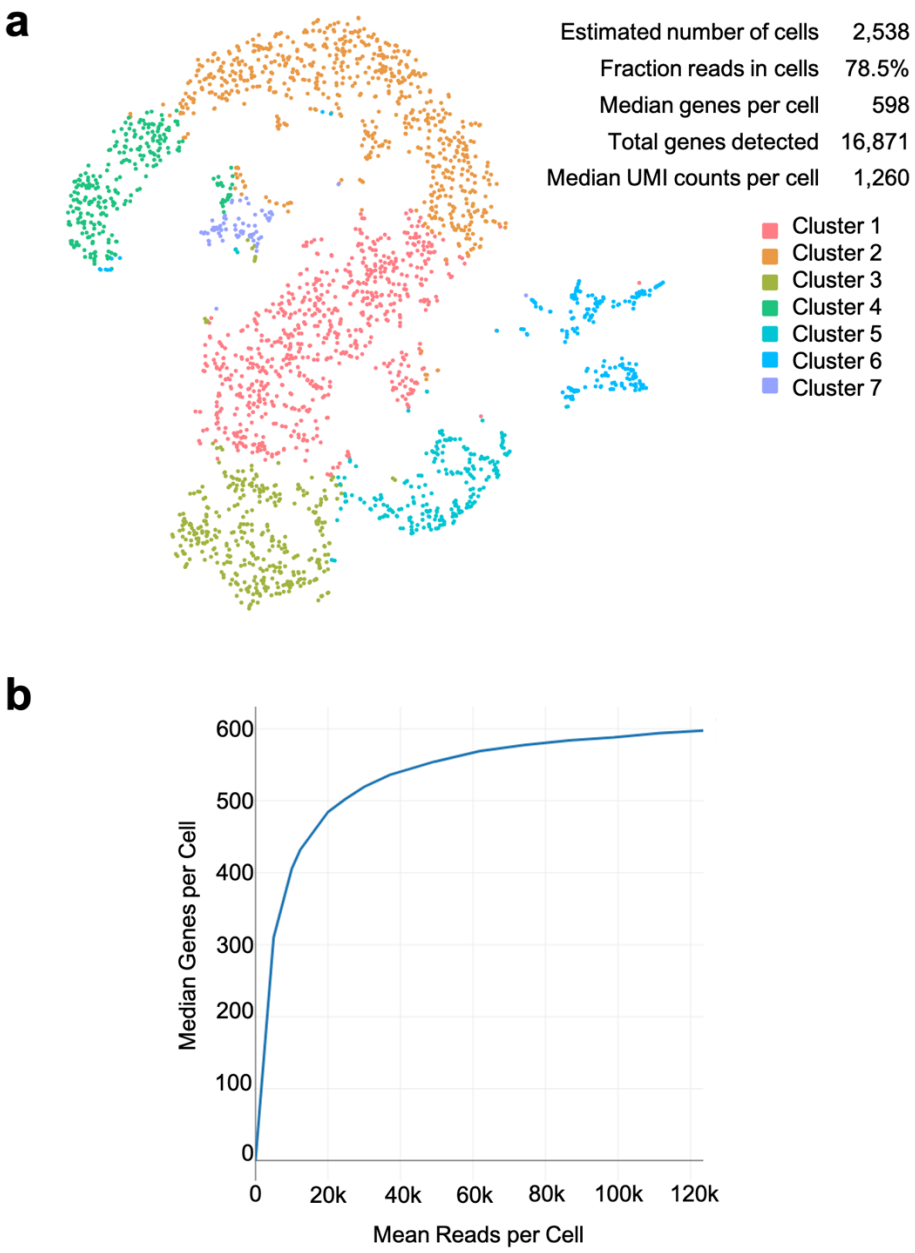

Supplementary Fig. 4: Cellranger clustering analysis of the 10X Genomics scRNA-seq of 2,528 pollen nuclei from *R. breviuscula*. (a) Clustering analysis identified 2,538 nuclei grouped in seven clusters composed of vegetative and generative pollen nuclei. **(b)** Curve showing the cumulative median number of genes per pollen nucleus as read coverage increase. Note the low median value of genes detected.

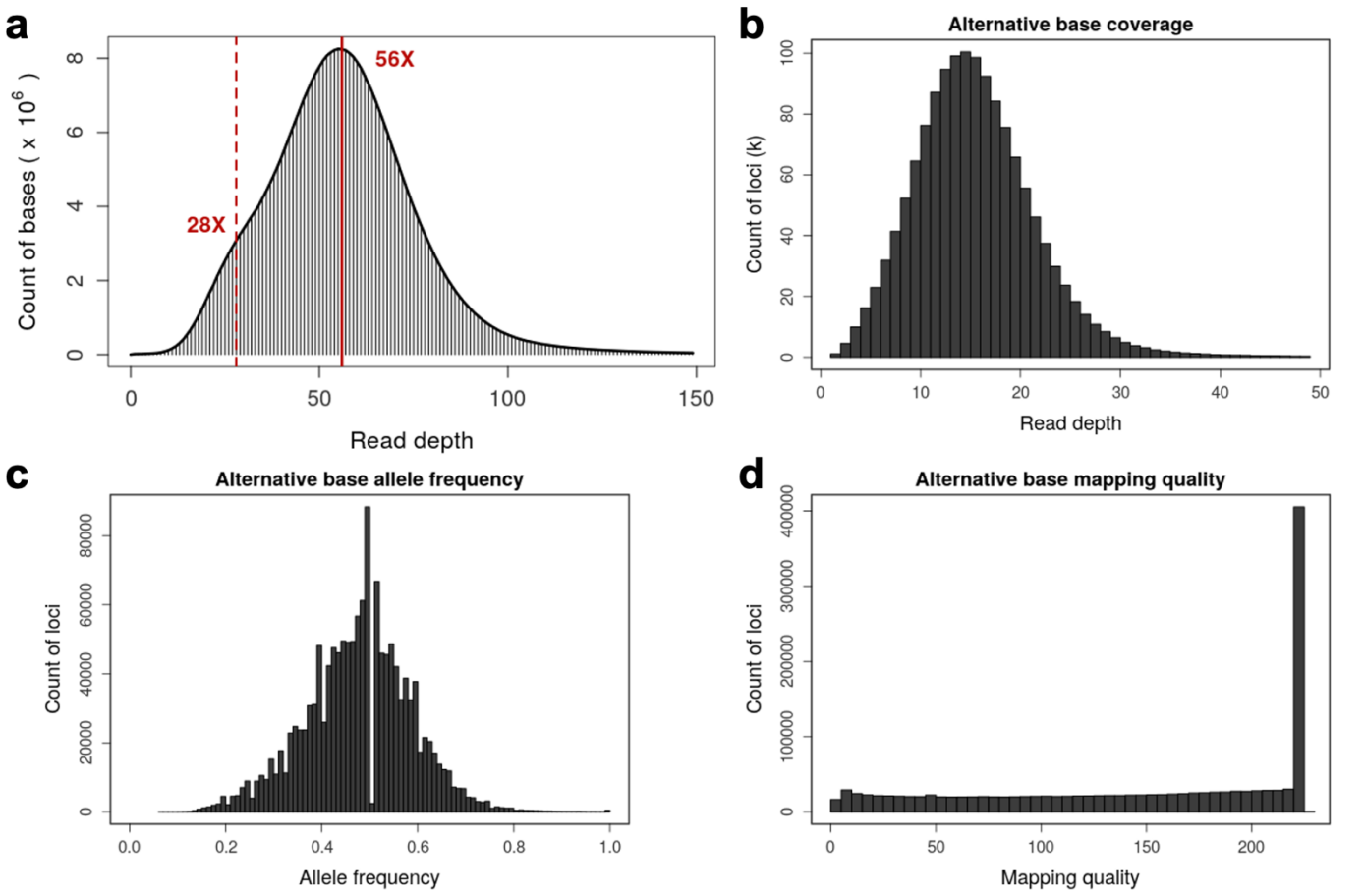

Supplementary Fig. 5: Selection of genotyping markers on the reference genome. (a) Distribution of read depth of Illumina reads mapping to haplotype 1 of the *R. breviuscula* phased genome. **(b–d)** Characteristics of alternative bases of SNPs that were called from the alignment mentioned in **(a)**. Genotyping markers on the reference were selected according to the distributions of coverage **(b)**, allele frequency **(c)**, and the mapping quality **(d)** of alternative bases. Specifically, an alternative base at a SNP position that met the requirements "5 ≤ alternative base coverage ≤ 30, 0.4 ≤ allele frequency ≤ 0.6, mapping quality > 50" was an allelic SNP, i.e., a genotyping marker.

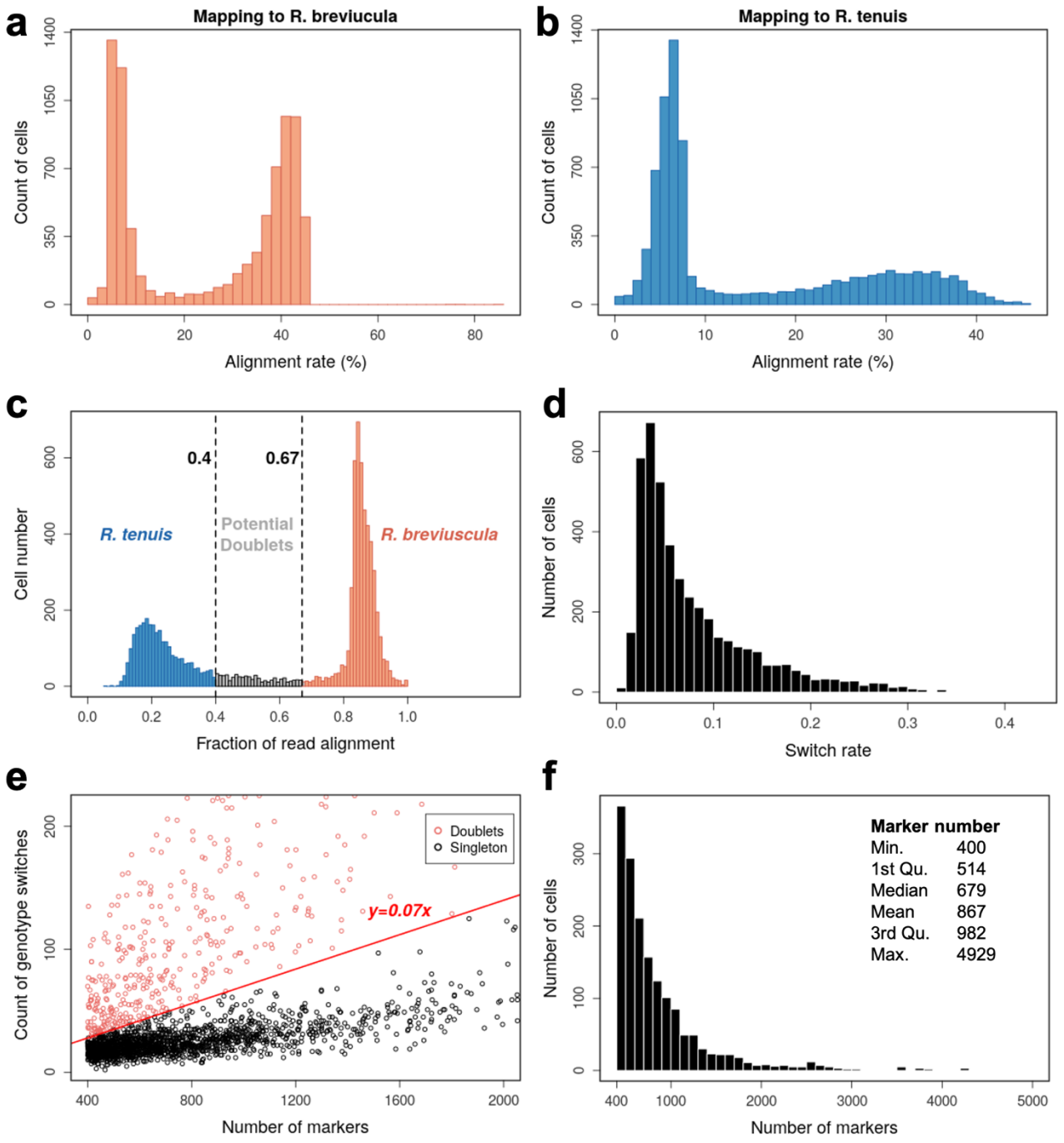

Supplementary Fig. 6: Pre-processing of scRNA-seq by separating *R. breviuscula* from *R. tenuis* cells and removing doublets. The scRNA-seq library was prepared with mixed pollen nuclei of *R. breviuscula* and *R. tenuis* for multiplexing purposes, thus it was necessary to discriminate the single-cell data between the two species at first. **(a–b)** Distribution of alignment rates of each read to *R. breviuscula* **(a)** and *R. tenuis* **(b)**. **(c)** Distribution of the fraction of reads from each cell aligning to *R. breviuscula* over the read alignments to both species, i.e., for a certain cell, fraction = number of reads mapped to *R. breviuscula* / (number of reads mapped to *R. breviuscula* + number of reads mapped to *R. tenuis*). Cells with an alignment fraction over 0.67 are potentially from *R. breviuscula*. Those with a fraction below 0.4 are potentially from *R. tenuis*. The remaining cells are doublets. **(d)** Distribution of switch rate across *R. breviuscula* pollens. The switch rate of a certain cell was calculated as the frequency of genotype switches between two consecutive markers over the total number of markers in this cell. **(e)** Identification of doublets by switch rates. Cells with a switch rate over 0.07 were considered doublets. **(f)** Number of markers across *R. breviuscula* pollen cells with a high number (≥400) of markers and no doublets.

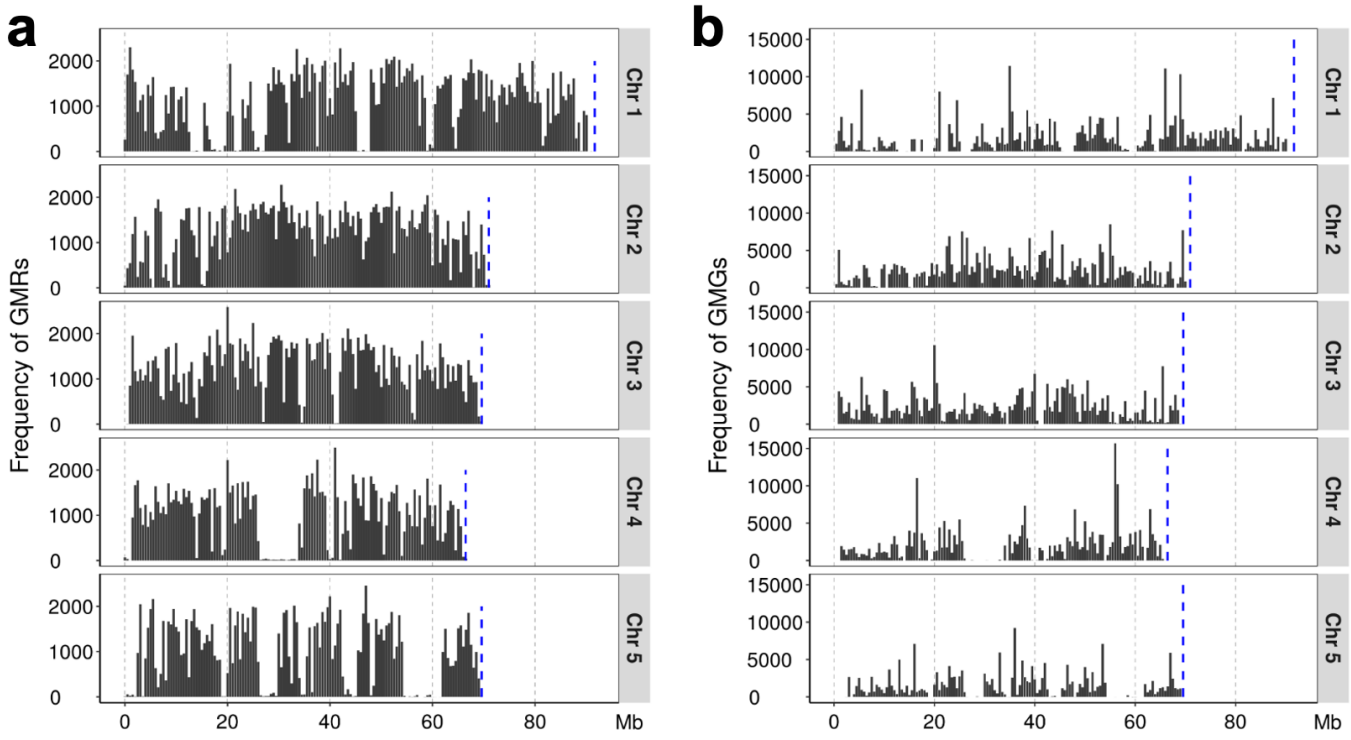

Supplementary Fig. 7: Marker distribution on the reference and across all viable pollen nuclei. (a) Frequency of genotyping markers defined along each chromosome on reference rhyBreHap1. Blue dashed lines show the end of each chromosome. GMR, genotype markers on reference genome. **(b)** Frequency of all markers across viable pollen nuclei that were used for CO detection. GMG, genotype markers on gametes.

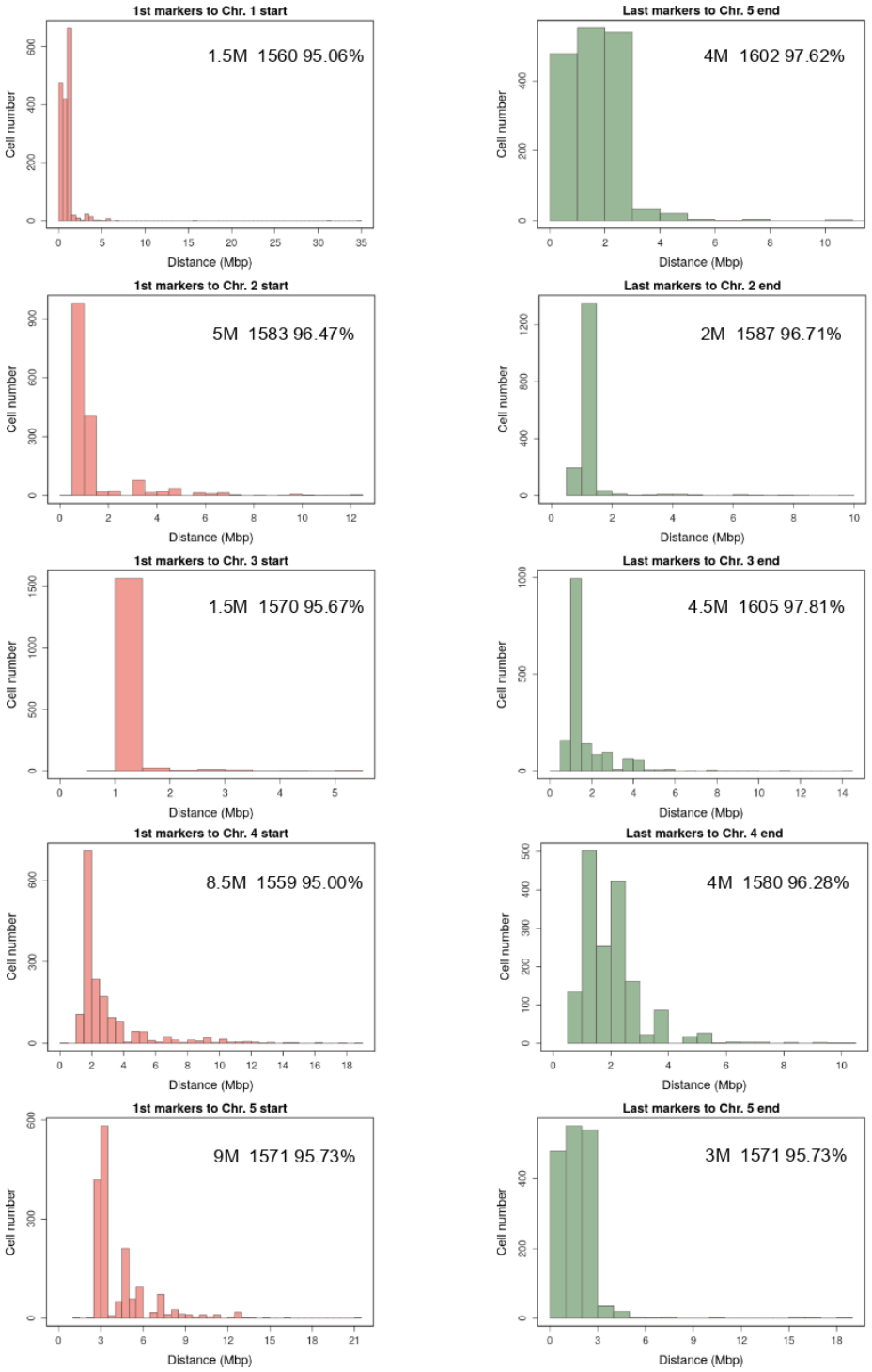

Supplementary Fig. 8: Distance distribution of the first markers to the chromosome start and the last markers to the chromosome ends across all viable pollen nuclei. If the regions covered by the first and last markers can be found in at least 95% of pollen nuclei, they are defined as confident start and end of the recombination landscape. The number on each plot indicates the distance of the confident regions to the chromosomal ends, the number of pollen nuclei covered, and the percentage of covered pollen nuclei.

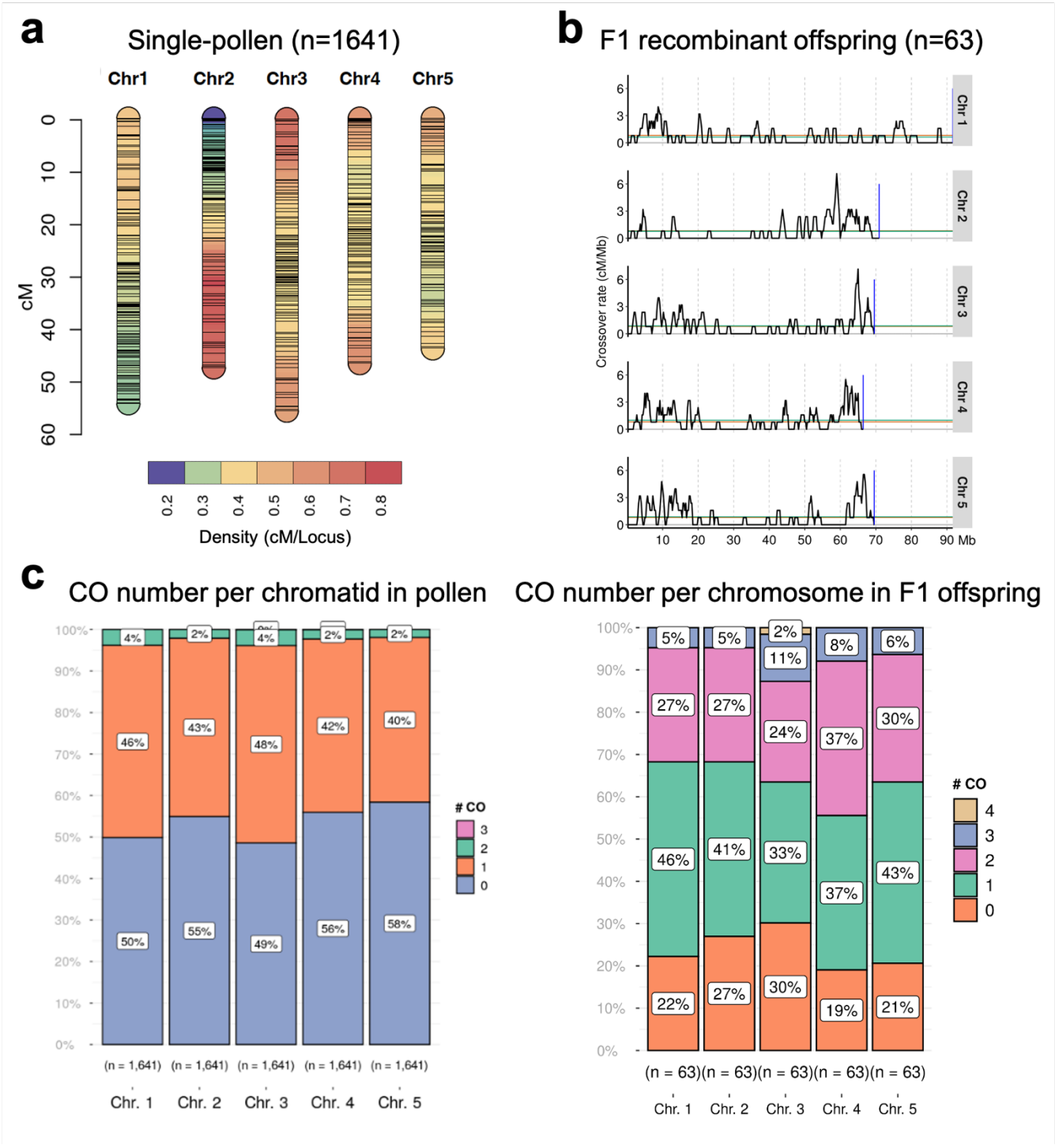

Supplementary Fig. 9: Comparison of recombination frequencies in the single-pollen sequencing data and in the F_1 recombinant offspring of *R. breviuscula*. (a) Genetic linkage map using COs detected in our 1641 pollen nuclei with density indicated by colouring. The 705 markers were selected using a 500-kb sliding window through all markers defined on the reference (**see Methods**). **(b)** Recombination landscape of the five chromosomes in *R. breviuscula*, determined by computing COs in 63 F_1 offspring individuals. Black line displays the CO rate. Blue solid vertical lines indicate chromosomal ends. Orange horizontal line: genome-wide mean CO rate. Green horizontal line: chromosome-wide mean CO rate. **(c)** Distribution of CO numbers across single chromatids in all 1,641 viable pollen nuclei (left) and in individual chromosomes in the F_1 offspring (right; N=63 F1 plants).

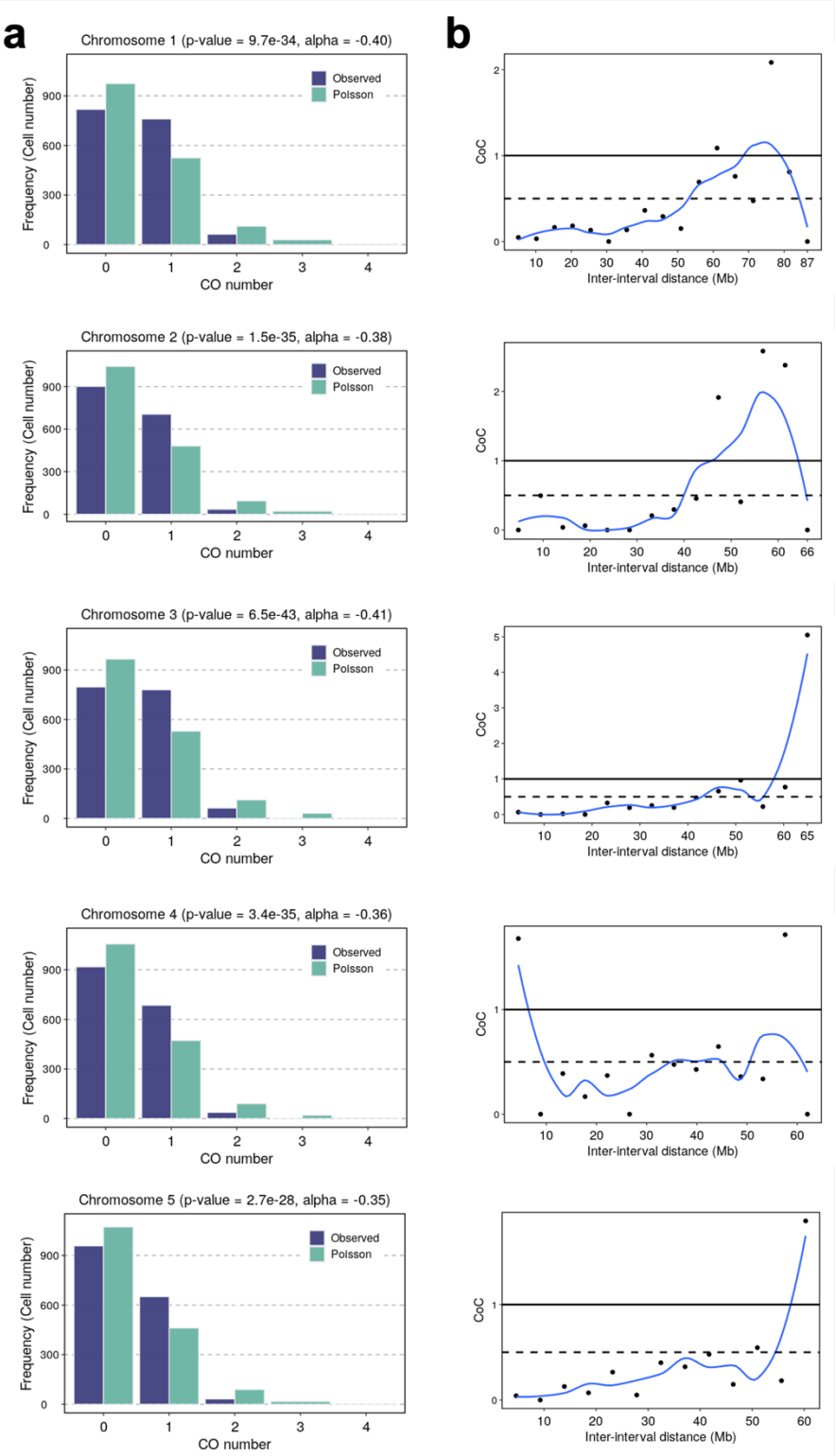

Supplementary Fig. 10: CO interference on each chromosome. (a) Comparison of observed CO number and expected CO number under the assumption of no interference on each chromosome. Chi-square values were first computed based on the chi-square goodness-of-fit test with a Poisson distribution. The *p*-value was computed based on a chi-square distribution with the above Chi-square value and degree of freedom. The alpha value was derived from the dispersion test. **(b)** CoC curve for each chromosome in the pollen nuclei (*n* = 1,641). Chromosome 1 was divided into 18 intervals and chromosomes 2–5 were divided into 15 intervals. Random sampling was performed on the CO intervals to calculate the mean CoC of each pair of intervals.

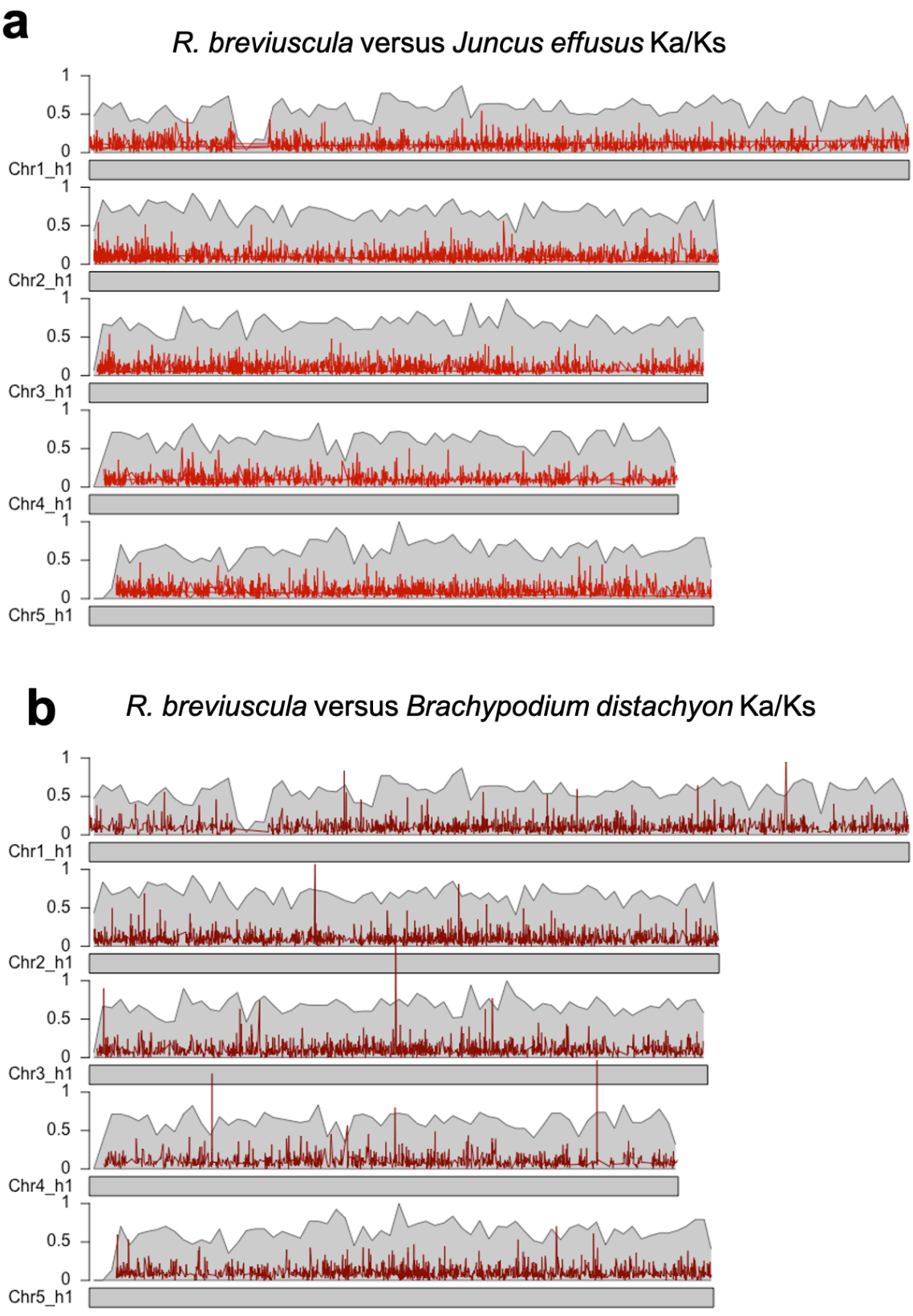

Supplementary Fig. 11: Ka/Ks ratio estimation across the chromosomes of *R. breviuscula*. **(a)** Ka/Ks ratio comparison between *R. breviuscula* and *Juncus effusus* genomes. **(b)** Ka/Ks ratio comparison between *R. breviuscula* and *Brachypodium distachyon* genomes. X-axis: gene start, Y-axis: Ka/Ks values; grey background: gene density. High Ka/Ks values indicate fast-evolving regions.

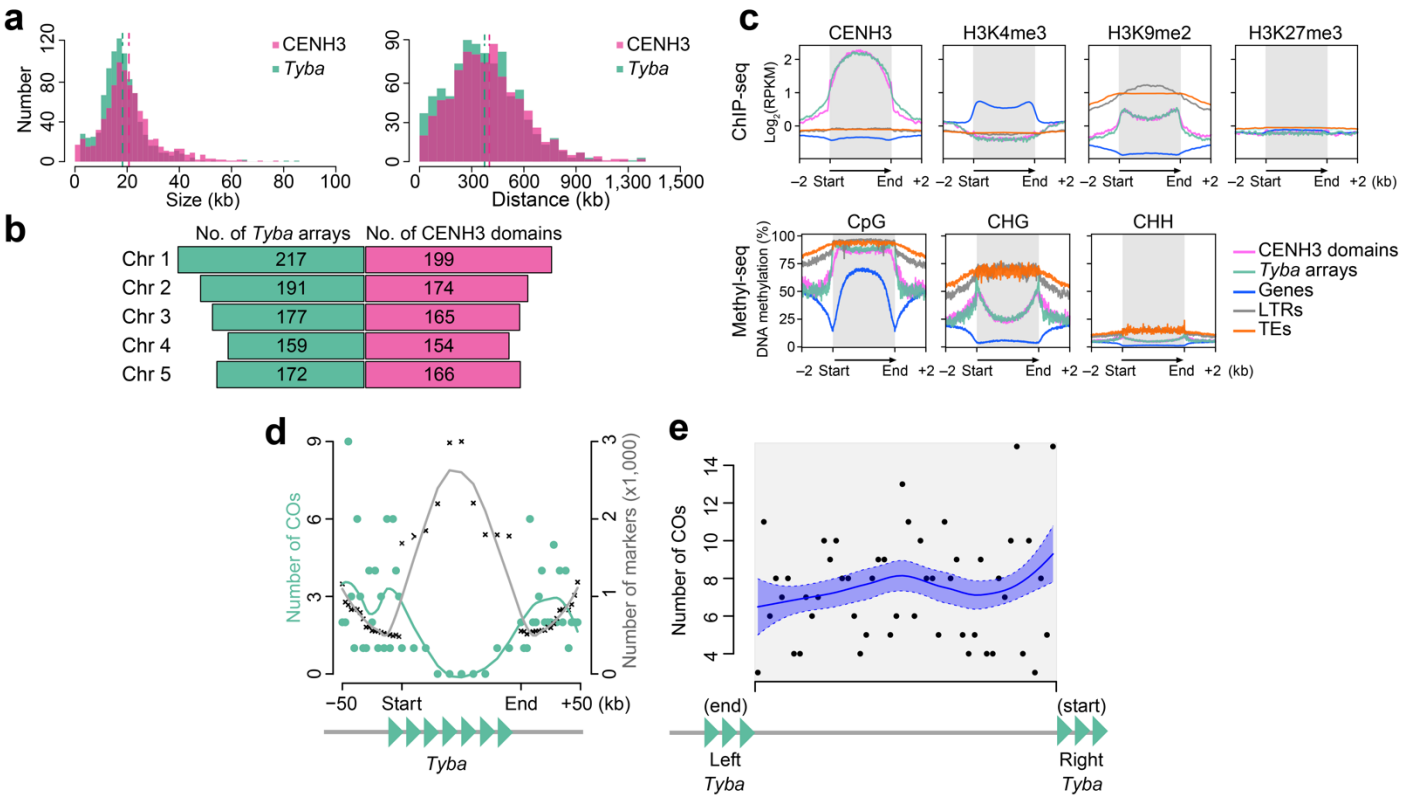

Supplementary Fig. 12: Epigenetic regulation of repeat-based holocentromeres and fine-scale correlation of CO positions with *Tyba* repeats. (a) Size (left) and spacing (right) length distribution of CENH3 domains and *Tyba* arrays. CENH3 domain median size is 19,156 bp and the mean size is 20,697 bp. The median of *Tyba* array size is 17,424 bp and the mean is 18,220 bp. CENH3 domain median spacing is 378,467 bp and the mean is 401,763 bp. The median of *Tyba* array spacing is 354,850 bp and the mean is 374,310 bp. **(b)** Number of *Tyba* arrays (left) and CENH3 domains (right) for each chromosome annotated in the reference haplotype genome. **(c)** Enrichment of CENH3, H3K4me3, H3K9me2, and DNA methylation in the CpG, CHG, and CHH contexts from the start and end of different types of sequences: CENH3 domains (magenta), *Tyba* repeats (green), genes (grey line), LTRs (yellow-green), and TEs (orange). ChIP-seq signals are shown as log2 (normalised RPKM ChIP/input). Grey boxes highlight the modification enrichment over the body of each sequence type. **(d)** Within *Tyba* arrays CO frequency is remarkably suppressed, despite relative high marker density. **(e)** Random distribution of the relative distance of CO positions to the end of the left and to the start of the right *Tyba* array. The median of CO resolution is 334 bp and the mean is about 2 kb. Correlation analysis performed using data from 63 F_1 recombinant offspring and a total of 378 COs. Green-filled triangles schematically represent *Tyba* repeat arrays.

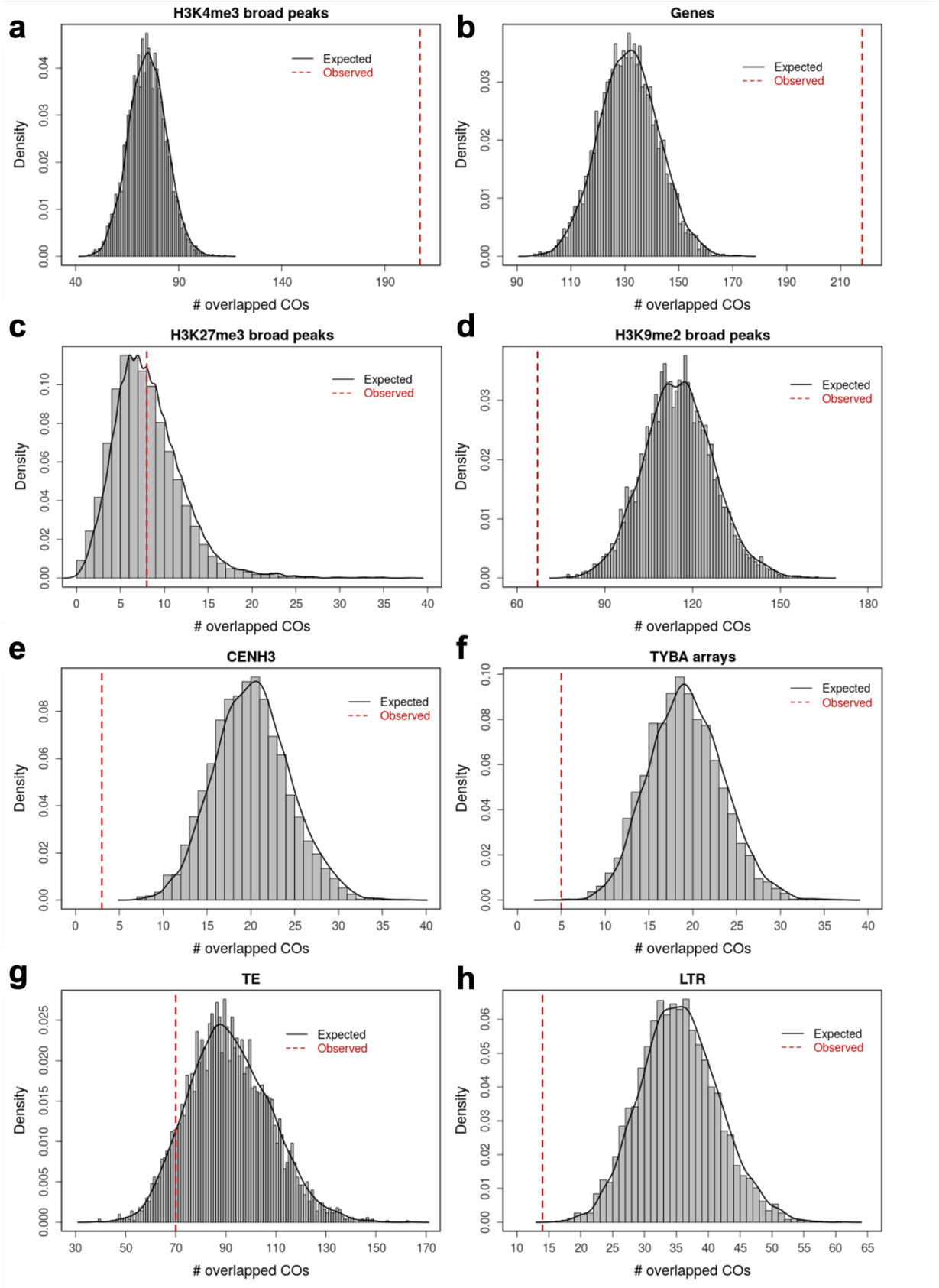

Supplementary Fig. 13: Comparison of numbers of COs overlapped with (epi)genetic features to random simulations. Observed overlapped CO number is displayed with red dashed vertical lines. Histograms show the distributions of overlapped CO numbers with H3K4me3 **(a)**, genes **(b)**, H3K27me3 **(c)**, H3K9me2 **(d)**, CENH3 **(e)**, *Tyba* arrays **(f)**, TEs **(g)**, and LTRs **(h)** in 5,000 simulations of randomly assigned COs.

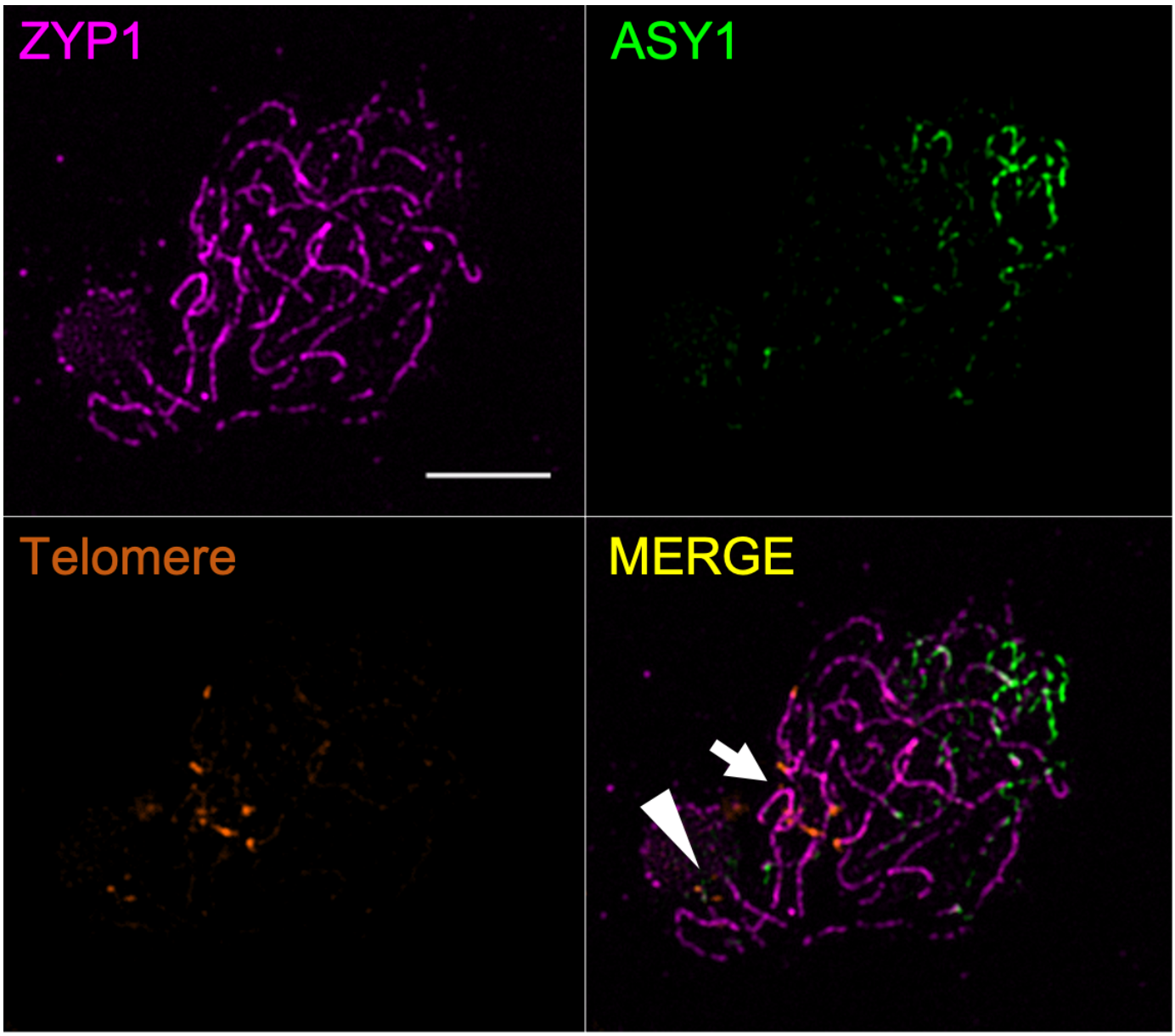

Supplementary Fig. 14: Immunolocalisation of ZYP1, ASY1 and telomere-FISH. In late zygotene, ASY1 (green) represents unsynapsed chromosomes not yet reached by ZYP1 (magenta), while ZYP1 occupies the rest of the chromosomal length loaded with the SC. Telomeres (orange) are still clustered in the *bouquet* (white arrow) or at the nucleolus (white arrowhead). Scale bar, 5 µm.

Zygotene

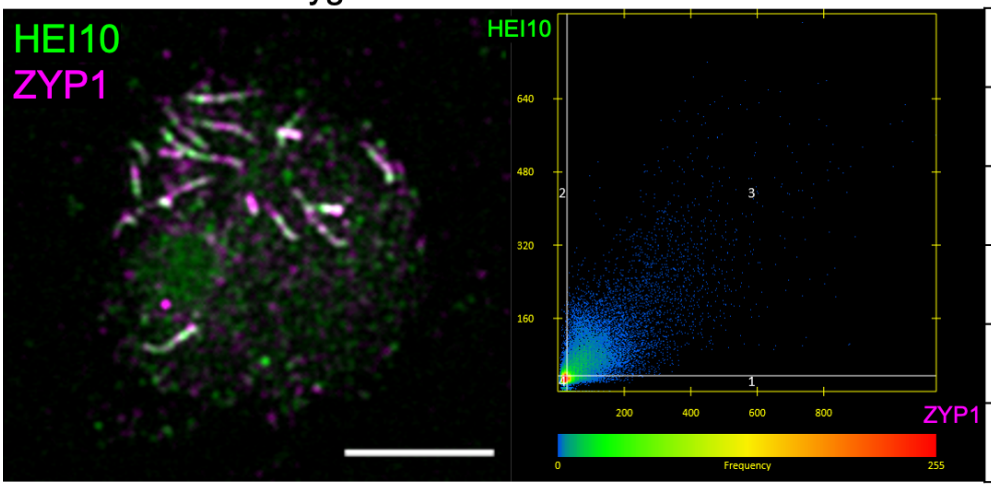

Pearson Coeff.	0.68437
Manders Coeff.	0.879
Coloc. Coeff. ZYP1	0.72302
Coloc. Coeff. HEI10	0.768
Weighted Coloc. Coeff. ZYP1	0.8609
Weighted Coloc. Coeff. HEI10	0.87287

Pachytene

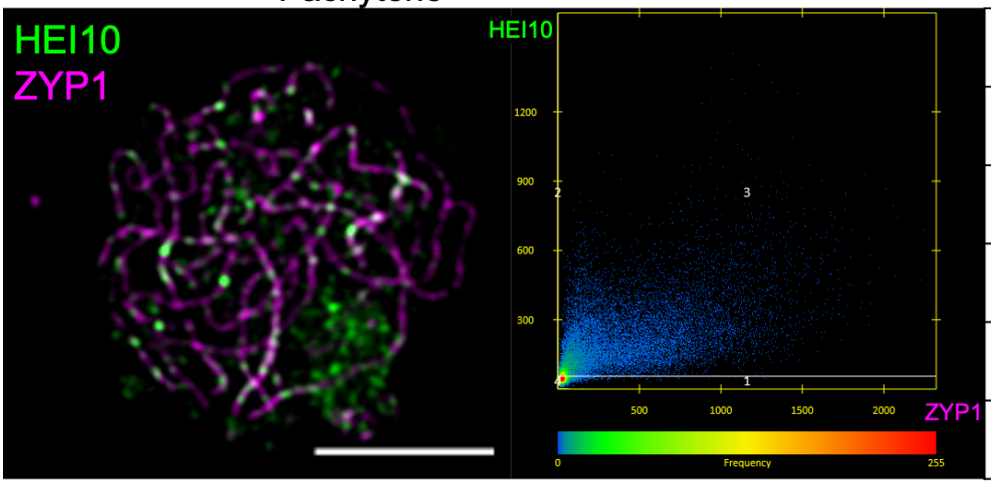

Pearson Coeff.	0.56351
Manders Coeff.	0.79553
Coloc. Coeff. ZYP1	0.57618
Coloc. Coeff. HEI10	1
Weighted Coloc. Coeff. ZYP1	0.92247
Weighted Coloc. Coeff. HEI10	1

Supplementary Fig. 15: Colocalization analysis of processed images of meiocytes at zygotene (top) and pachytene (bottom). The analysis shows a positive and non-random colocalization between HEI10 and ZYP1 signals. This behaviour was consistent among all cells analysed at either zygotene or pachytene stage (N=44). Images were processed with ZEN software (Zeiss), utilizing the colocalization function. Intensity threshold was automatically selected by Costes significance algorithm.

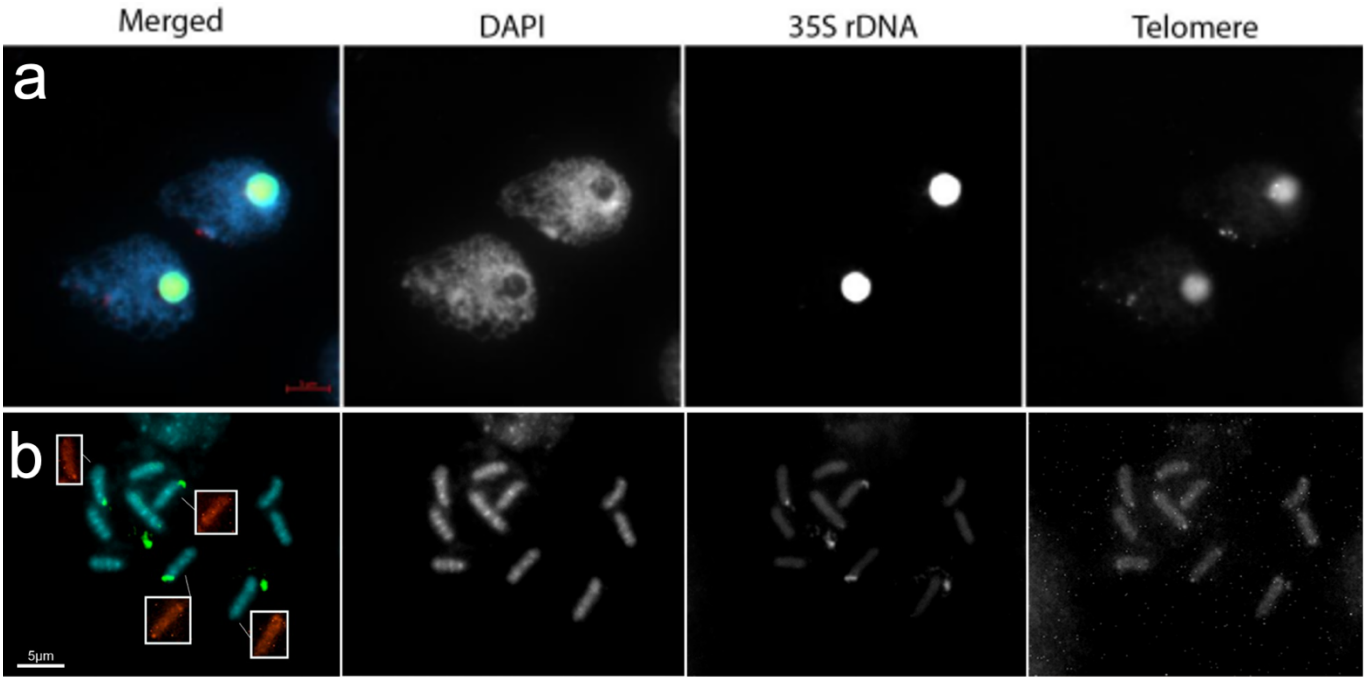

Supplementary Fig. 16: FISH with *35S rDNA* and a telomeric probe in *R. breviuscula*. Prophase I **(a)** and mitotic metaphase **(b)**. Telomeres of the *rDNA*-harbouring chromosomes 1 and 2 cluster in the nucleolus. Squares in **b** show telomeric sequences in chromosomes with 35 rDNA. Scale bar, 5 µm.